$\mathcal{D}14$

ANALYSIS OF LIQUID DYNAMICS FOR M551 AND M553 SKYLAB SPACE PROCESSING EXPERIMENTS

M. R. Brashears, S. V. Bourgeois, C. Fan
Lockheed Missiles & Space Company, Inc., Huntsville, Ala. 35807

ABSTRACT

Fluid mechanic analyses were performed for the M551 and M553 materials processing experiments developed by NASA-Marshall Space Flight Center and conducted in the M512 facility aboard the Skylab laboratory by Astronaut Charles Conrad. The M551 Metals Melting experiment consisted of three sample disks with varying thicknesses. An electron beam gun was used to produce a weld seam as well as a molten pool in each specimen which was made to rotate at a controlled speed. The M553 Sphere Forming experiment consisted of 28 nickel specimens of 6.35 mm diameter being cast by utilizing an electron beam as the heat source. After melting, the molten spheres were designed to separate and solidify under a free-float condition in the vacuum chamber.

The beading and spiking phenomena in the M551 experiment are discussed. An analysis of the beading phenomena based on the Kármán vortex shedding theory is presented. A dynamic model of cavity oscillation is discussed to explain the spiking phenomena which were observed in the stainless steel and tantalum samples. The intensity of spiking depends primarily on the vapor pressure and surface tension properties of the material. Spiking may also be affected by the level of gravitational acceleration, however, at low degrees of melt superheat.

Both order-of-magnitude dimensional analysis and thermoconvective instability (perturbation) analysis are applied to the molten metal droplets of the M553 experiment. The controlling physical forces and magnitude of fluid flow are predicted and compared to results exhibited on high-speed photography. Convection thereby ascertained is utilized to analyze expected low-g effects on the attendant solidification processes.

For both experiments, particular emphasis is placed on clarifying the effects of reduced gravity on molten metal flow and solidification.

INTRODUCTION

The M512 facility was flown aboard the Skylab Laboratory to provide the working chamber for numerous scientific experiments including several space processing experiments. The facility included an electron beam heat source operated from 50 to 80 mA at 20 kV aligned in a 40 cm diameter chamber vented directly to outer space. The M551 metals melting and the M553 sphere forming experiments were performed during the June 1973 mission by Astronaut Charles Conrad.

The M551 experiment consisted of three sample disks, each containing three metal specimens of varying thicknesses. These disks were rotated automatically at a controlled speed of 2.5 rpm under an electron beam gun with the gun targeted to produce an electron beam weld seam in

each specimen at a radius of 6 cm. Disk materials included 2219 aluminum, 321 stainless steel and tantalum. During the continuous weld portion of each disk both full and partial penetration of the disk was achieved by having a constant power input with a varying disk thickness. For each disk, the continuous weld was followed by a dwell portion. In the dwell portion of the weld, the disk was stationary, allowing the electron beam to impinge on a thick segment of the disk, thus creating a large molten pool. The electron beam was then cut off to allow the pool to solidify.

The M553 experiment consisted of twenty-eight 6.35 mm diameter spherical specimens cast by utilizing the electron beam heat source. Initially, cylindrical specimens were supported on two wheels (14 specimens on each) by a sting. During melting, spherical drops were formed and subsequently designed to be released from their stings and allowed to solidify while free floating in the vacuum chamber. Specimens consisted of pure nickel, Ni-1% Ag, Ni-30% Cu and Ni-12% Sn.

During the course of the investigation all process phenomena were considered with particular emphasis on the melting and solidification of metals in reduced gravity. Included in these analyses were detailed studies on the fluid dynamics of the molten metal.

For these particular Skylab experiments, the only significant difference between space and earth processing was the lack of gravity. The maximum gravity level experienced during operation of the M551 and M553 experiments aboard Skylab II was 7×10^{-4} g_E (g_E = 9.8 m/sec^2). Other environmental factors which may also differ from earth processing are the vacuum, radiation, electromagnetic and thermal conditions.

Gravity has no direct effect on grain structure or other properties of solidified material. These properties are determined by the crystallization kinetics which are controlled by short-range intermolecular forces; i.e., the temperature and concentration at the fluid-solid interface. Gravity has not been shown to have any significant direct effect on these forces, but can affect solidification indirectly through its direct effect on fluid motion. The three major indirect effects of gravity on solidification are:

- Sedimentation

- Buoyancy-Induced Convection, and

- Hydrostatic Pressure.

These mechanisms are all hydrodynamical in nature. Detailed discussions of the objectives of the study, as well as the results, are available in Refs. 1 through 3.

M551 METALS MELTING EXPERIMENT

- Convection Effects on Solidification

Cross-sectional micrographs of the M551 aluminum disks (Fig. 1) indicate that grain size and orientation differed appreciably between the ground and Skylab samples. Similar trends were exhibited by the stainless steel and tantalum specimens. The ground-based sample consists of large, columnar grains growing normal to the unmelted solid with slight evidence of banding. The Skylab

sample, however, is fine grained and equiaxed. One other significant differ-
ence is the negligible width of the chill zone (ultra-fine grained, equiaxed region
adjacent to the parent metal) in the ground sample.

Some investigators have attributed these differences to reduced convec-
tion during Skylab processing. The accepted principles of crystal growth (Ref.4)
however, lead to the opposite conclusion. Many experiments have now shown
the strong effect of convection on grain size in cast metals. When this convec-
tion is reduced, grain size is larger and columnar structures are much more
readily obtained. Convection also appears to play a dominant role in formation
of the chill zone as well as in the columnar-equiaxed transition. When convec-
tion is absent, no outer chill zone is observed.

One other possibility for the results shown in Fig. 1, besides differences
in convection,would be the degree of superheat supplied to the ground and Skylab
samples. Superheating results in coarser structures (Ref. 5, p. 6). Thus, the
fine grained Skylab structure would indicate less superheat, but its melt zone
was 18% greater than the ground sample which indicates higher superheat on
Skylab or greater convection on Skylab.

Thus, increased convection during Skylab processing (rather than reduced
flow) explains the different microstructures observed in the micrographs, Fig. 1,
of the M551 aluminum disk. Preflight analysis predicted an equivalent magni-
tude of convection between terrestrial and Skylab processing (Refs. 2 and 3).
Increased convection aboard Skylab can be explained if the gravity driven and
Marangoni convective flow patterns tended to oppose each other on earth. This
would leave the unopposed Marangoni convection aboard Skylab to be more vig-
orous throughout the melt zone. Furthermore, the spiking mechanism is ex-
pected to give rise to increased stirring aboard Skylab.

● Beading Phenomenon

During the M551 experiment, motion pictures were taken for each of the
three metal disks. The motion pictures taken along with the experiment speci-
mens were then brought back to earth for analysis. Shown in Fig. 2 are photo-
graphs taken of the 321 stainless steel after being subjected to electron beam
impingement in the flight and ground experiments. For comparison purposes,
ground-based tests were also made of the same specimens under similar operating
conditions. The photographs taken for the three M551 materials during ground
tests are shown in Ref. 6. The most striking phenomenon appearing in these
photographs is the "beading" effect which occurs simultaneously with total eb
penetration in the stainless steel and tantalum specimens. No beading is ex-
hibited in the aluminum sample, however.

It was hypothesized (Refs. 1 and 3) that the forming of beads after the
passage of an electron beam was related to the vortex shedding phenomenon.
When a cylinder moves through a fluid above a certain speed, the cylinder sheds
behind its wake a periodic pattern of vortices which move alternatively clock-
wise and counterclockwise. This vortex formation is known as Kármán vortex
street. A sketch showing the streamlines of a Kármán vortex street is given in
Fig. 3. In this sketch, λ is the wave length or vortex spacing and h is the sepa-
ration distance between the two rows of vortices.

The shedding frequency, f, i.e., the number of vortices shed per unit time, is dependent upon the density, ρ, and viscosity, μ, of the fluid, the diameter of the cylinder, D, and the velocity, V, with which the cylinder moves relative to the fluid. The interrelationship between these quantities can be correlated in terms of two dimensionless parameters known as Strouhal number, S, and Reynolds number, R, which are defined as

$$S = \frac{f \times D}{V}$$

$$R = \frac{\rho\,V\,D}{\mu}\,.$$

The relationship between S and R was obtained experimentally (Ref. 6) for a fluid in large extent.

The wave length of the vortices, λ, is given by

$$\lambda = \frac{V - v}{f} \qquad (1)$$

where v is the velocity of the vortex which decreases with the distance from the cylinder. The magnitude of v is only of the order of 4 to 5% of V at a distance of 10 to 20 diameters downstream of the cylinder. The value of v is even smaller when the flow is confined by side walls. For all practical purposes v can be neglected in Eq. (1).

With the above basic background information, one can compile a list of data regarding the M551 space flight and ground-based experiments in view of the vortex shedding hypothesis. The compiled data are tabulated in Table 1. The manner in which these data are obtained is described as follows.

The two temperatures selected for calculation for each of the three M551 specimens correspond to the melting temperature and predicted maximum temperature (Ref. 1). The Reynolds number was calculated based on the velocity of the electron beam relative to the disk, the focusing diameter of the electron beam, and the density and viscosity of the molten metal. The viscosity of liquid metals depends strongly on temperature. The following equation was used in computing the viscosity of the molten metals

$$\mu = \mu_o\, e^{E/\Re T} \qquad (2)$$

where μ_o is a reference viscosity, E is the activation energy, $\Re$ is the universal gas constant, and T is the absolute temperature. The values of μ_o and E are different for different materials. For example, for the stainless steel specimen, μ_o and E_o are estimated to be (Ref. 7)

$$\mu_o = 0.37 \quad \text{Centipoise}$$
$$E = 9.9 \quad \text{Kcal/gm-mole-}^\circ\text{K}$$

After the Reynolds number was calculated, the Strouhal number was derived from Ref. 6. The shedding frequency can then be computed from the definition of the Strouhal number. The theoretical bead spacing (i.e., wave length)

is calculated from Eq.(1) by neglecting v. The data listed in the last two columns of Table 1 are the average bead spacings obtained by direct measurements from photographs.

It is seen in Table 1 that except for the aluminum specimen for which no beads were observed, the predicted bead spacing based on the vortex shedding theory and the experimentally measured average bead spacing are in good qualitative agreement. Quantitative agreement was not expected since the geometry and boundary conditions of the M551 Metals Melting experiment were not quite the same as those for a long solid cylinder moving in a fluid of large extent.

The theoretically predicted shedding frequency for each of the three specimens is also compared in Table 2 with corresponding experimental results for both space flight and ground-based tests. Again, good qualitative agreement among the data is obtained, except for the aluminum specimen.

It is theorized that surface tension must play an important role in the formation of beads from the vortices of the liquid metal during cooling and solidification. The larger the surface tension, the more easily the beads can be formed. The magnitude of surface tension (σ) for the three M551 materials at their respective melting temperatures are: (1) 321 stainless steel, σ = 1750 dyne/cm; (2) 2219 aluminum, σ = 737 dyne/cm; and (3) tantalum, σ = 2150 dyne/cm.

It is noted that the surface tension of 2219 aluminum is only 30 to 40% of that of the other two materials. Thus, it is quite possible that during the flight and ground tests with the 2219 aluminum specimen, vortices were present but no beads were formed due to insufficient surface tension force.

The above analysis is, of course, qualitative. The motion of the molten metal in the wake of an electron beam is influenced by many factors. In addition to the parameters involved in the definitions of Strouhal and Reynolds numbers, the state of the fluid motion is influenced by the thickness of the disk, confining side walls (between molten and solid metals), free surface and surface tension effects, as well as nonuniform temperature distributions.

In general, the effect of confining side walls is to increase the critical Reynolds number for the onset of vortex shedding. According to Taneda (Ref.8) when the ratio of the diameter of the cylinder to the distance between the walls is increased from 0 to 0.5*, the critical Reynolds number is increased from 45 to about 80. Shair et al. (Ref. 9) have also conducted experiments showing the effect of confining walls on the stability of the wake behind a circular cylinder. Their results indicated a more pronounced effect than that reported by Taneda. This may also explain the absence of beading in the aluminum specimen, since the calculated minimum Reynolds number for this case is only about 50. It appears, however, that confining wall effects alone do not explain the quantitative differences between the predicted and measured values of λ and f as tabulated in Tables 1 and 2.

---

* The ratio of the diameter of the electron beam to the width of the welding in the M551 experiments is approximately 0.5.

A recent literature search on the subject of vortex shedding revealed little information regarding the effects of the finite length of the cylinder in the low Reynolds number flow region. At high Reynolds numbers (R >1000), a shorter cylinder results in larger vortex spacing (Ref. 10). No information is found at all regarding nonuniform temperature and heat transfer effects on vortex shedding. A detailed analysis of these problems would certainly be very interesting.

● Spiking Phenomenon

A detrimental aspect sometimes inherent in electron beam welding is the phenomenon known as spiking which results in surface ripples and banding in the weld seam microstructure. Many examples of this effect have been documented, especially for partial penetration welds in stainless steel (Ref. 11). This phenomenon is caused by oscillation of the melt.

Several possible evidences of its occurrence during the M551 experiment have appeared in both the aluminum and stainless steel samples. Detailed descriptions of the causes and effects of spiking are given in Refs. 2 and 12.

The spiking frequency can be approximated by (Ref. 12).

$$\omega = \frac{\frac{1}{4}\sqrt{\frac{g}{h}}}{\sqrt{\dfrac{P_V - 2\sigma/a}{\rho g h}}\ \sqrt{\dfrac{P_V - 2\sigma/a - \rho g h}{\rho g h}}} \tag{3}$$

where

ω = spiking frequency

h = maximum depth of penetration

$2a$ = weld width

g = gravity level

P_V = vapor pressure of molten metal

σ = surface tension of molten metal

While the preceding equation should not be expected to generate exact, rigorous results to match actual M551 experimental data, it can be utilized to predict a low gravity variation in the spiking behavior of M551 materials. It can also be utilized to assess the effects on spiking of the degree of superheat. Increasing superheat lessens surface tension and density while increasing vapor pressure. Overall, increasing melt temperature through superheating should increase the spiking frequency. This is illustrated by examining Eq. (1) in the limit as g→, 0

$$\omega = \sqrt{\frac{P_V - 2\sigma/a}{4\rho h^2}} \tag{4}$$

which means that spiking cannot occur below $2027.^\circ C$ for stainless steel. The

surface tension force overcomes any jetting due to vaporization at lower surface temperatures. This is indicated by imaginary numbers in Eq. (4).

The effect of superheat and gravity on spiking frequency for all three M551 materials is shown in Figs. 4, 5 and 6. Physical property data were obtained primarily from Refs. 13, 14 and 15. These results indicate that: (1) spiking frequency varies inversely with gravity, but only above 10^{-2} g; (2) at large superheating, spiking becomes insensitive to microgravity-terrestrial gravity variations; (3) spiking occurs in the stainless steel melt above $600^\circ C$ superheat (melt temperature, $T_M = 1427^\circ C$); (4) spiking occurs in aluminum above $1000^\circ C$ superheat ($T_M = 643^\circ C$); (5) spiking occurs in the tantalum melt above $1300^\circ C$ superheat ($T_M = 3000^\circ C$); (6) Skylab stainless steel samples are most prone to spiking. At minimum degrees of superheating, spiking frequency may be increased by 50% when g-levels of 10^{-4} are attained. This translates to a spike separation distance of 1.1 mm on ground tests versus 0.7 mm on Skylab.

Previous thermal calculations indicate that $600^\circ C$ of superheat at the melt surface are easily attainable (Ref. 1, p. 26) in the stainless steel specimens, while a superheat of $1000^\circ C$ for aluminum is also feasible (Ref. 1, p. B-4). It is doubtful that spiking temperatures were achieved in the tantalum specimens (Ref. 1, p. B-14). Thus the ripples on the aluminum and the ripples in the stainless steel microstructure may be caused by spiking.

One additional qualitative assessment can be made for the M551 aluminum specimens, i.e., the apparent disappearance of ripples in the weld region behind the molybdenum film. The molybdenum film has a dimension of 0.5 x 0.5 x 0.0005 inch and was placed on each of the M551 samples in the weld path at a location of 240 degrees. The purpose of placing a molybdenum film on each sample was to analyze fluid motion during melting by micro-sectioning of the weld.

The molybdenum has a lower total vapor pressure and increased surface tension forces (Refs. 14 and 16), thereby decreasing the tendency toward spiking.

● Conclusions

Analyses of both the space flight and ground-based tests of the M551 Metals Melting experiments indicate that:

- ● Good qualitative agreement was obtained between the measured results of beading frequency and spacing and the predicted values based on the Kármán vortex theory. This tends to support the hypothesis as advanced in Ref. 1 that the beading phenomenon which occurred in the stainless steel and tantalum samples was a Kármán vortex street formation.

- ● Surface tension and sidewall effects appear to be responsible for the absence of beadings in the 2219 aluminum sample after electron beam impingement.

- ● Reduced convection in space is definitely not the cause of altered microstructures found in Skylab 2219 aluminum.

- ● Altered or increased convection can explain the different microstructures exhibited by the Skylab 2219 aluminum specimen; i.e., Skylab convection dominated by surface tension forces whereas ground-based convection controlled by a combination of surface tension and gravity forces.

- Spiking frequency varies inversely with gravity, but only above 10^{-2}g.

- At large superheating, spiking frequency is independent of gravity.

- Stainless steel is the M551 material most prone to spiking, and its spiking frequency may be increased by 50% when g-levels of 10^{-4} are attained.

- Disappearance of surface ripples beyond the molybdenum patch on the ground aluminum samples can be attributed to molybdenum's inherent physical properties which tend to reduce or eliminate spiking.

M553 SPHERE FORMING EXPERIMENT

The fluid dynamics of the M553 experiment is an important factor in determining the quality of the final product. Flow patterns in the molten materials are important because all of the sample materials have low entropies of fusion (Ref. 17). Thus, their solidification (microstructure) is controlled by the rate of heat transfer removal (Ref. 18), which changes with the fluid flow (Refs. 19 and 20). The degree of flow will also determine the amount of mixing attained. Fluid flow can also affect the shape and release of the specimen while it is retained on the ceramic holder.

Application of dimensional analysis (Refs. 21 and 22) to the governing equations for eb melting, coupled with ground-based experiments, enabled prediction of the extent of reduction or increase of motion in the molten metal and/or the change in flow pattern in electron beam melting in space. Possible physical forces which could induce fluid flow in the M553 experiment and their causes include:

- Effective Gravity Force: Resultant force on weld specimen due to earth's gravity and centrifugal and coriolis forces of orbiting spacecraft.

- Lorentz Force: Electromagnetic forces induced by passage of the electron beam current through the specimen.

- Electrostriction: Stresses induced when electrical permittivity changes with density.

- Magnetostriction: Stresses induced when permeability changes with density.

- Electrostatic Force: Caused by presence of excess electrical charge.

- Surface Tension: Tangential stresses at vapor-liquid interfaces can be induced by nonuniform heating or impurities because surface tension depends on temperature and concentration.

- Shrinkage Force: Density differences accompanying phase changes usually cause flow inward to a growing solidification interface.

- Beam Force: Impinging electrons giving up their momentum.

- **Thermal Expansion:** Dilation and compression of fluids whose density changes appreciably with temperature can induce fluid flow.

- **Vibration:** Uncontrolled movement due to engine operation, astronaut motion, particle impacts, etc.

- **Centrifugal and Coriolis:** Generated by disk rotation.

- **Vapor Pressure:** Evaporating molecules impart momentum which leads to normal stresses at vapor-liquid interface.

- **Inertia Forces:** Tend to sustain existing motions and resist changes in flow.

- **Viscous Forces:** Tend to resist driving forces.

The preceding forces, which could influence fluid flow and solidification, appear explicitly in the conservation equations (Ref. 3) which apply to formation of a molten pool by electron beam heating. The controlling forces were previously determined via nondimensional and order-of-magnitude analyses (Ref. 2). The most significant results found are summarized below:

- **Vigorous convective stirring** occurs in the molten metal for each of the M553 sample materials. This fluid motion was exhibited on high speed motion picture film taken for ground tests and low gravity KC-135 aircraft tests.

- Both gravity and surface tension forces control molten metal flow during M553 ground tests. These natural convection driving forces arise because of severe nonisothermality during heating.

- Surface tension driven convection occurred in Skylab electron beam melting. In the near absence of gravity, the surface tension forces provided an equivalent amount of convection aboard Skylab, but the flow pattern might have been different from those of operations on earth.

- Velocities of 20 cm/sec magnitude were attained 0.1 sec after melting began in the M553 nickel specimen (both for Skylab and ground tests). Fluid flow decayed 60 seconds after melting began. This means that some degree of flow existed upon freezing even for the free-floating M553 spheres.

The effects on fluid motion of surface free charges (excess electrostatic charge) and related electric and magnetic forces at the drop surfaces were also examined. These surface charges are negligible driving forces for fluid motion (Refs. 23 through 25). Furthermore, from the manner in which patches of surface contaminants moved about in the ground films, it is apparent that surface tension driven flows due to concentration gradients may also have been important in this experiment. No reliable data exist, however, on what these impurities are, nor what the value of surface tension gradient with composition is. Thus, the Marangoni effects were limited to thermal differences only in this study.

Application of an earlier analysis of Marangoni thermoconvective stability in drops by Bupara (Ref. 26) yields the same conclusion as to convection in zero gravity. Bupara's study consisted of a steady-state perturbation analysis on

internally heated drops. Thus, his results do not rigorously apply to the rapid heating of the M553 experiment, but allow for an interesting comparison with dimensional analysis. His stability curve (see Fig. B5.1, Ref. 26) indicated a critical Marangoni, Ma_c, of 150. Upon release from the ceramic pedestal, the molten nickel spheres will possess the following properties: $R = 0.3175$ cm, $d\sigma/dT = 0.4$ dyne/cm-^oC, $\rho = 7.77$ g/cc, $\mu = 0.05$ g/cm-sec, $k = 0.15$ cal/cm-sec-^oC, $C_p = 0.157$ cal/g-^oC, $\beta = 10^{-4}/^oC$ and $dT/dr = 4450^oC$/cm (assuming no convection, Ref. 1). Defining Marangoni number as

$$M_a = \frac{-\rho\, C_p \frac{d\sigma}{dT} \frac{dT}{dr} R^2}{\mu k}$$

one obtains $Ma/Ma_c = 29100/150 = 200$, which indicates vigorous convective stirring. Several seconds after release the temperature gradient reverses and becomes -3.4^oC/cm after rapid equilibration (assuming no convection). This gives $Ma = -71$.

● Conclusions

   The primary conclusion of the preceding discussions is that significant flow and stirring in the molten spheres (during and after eb melting) occurred in both terrestrial and space processing as predicted. The magnitude of this convective fluid motion was the same in both environments.

   Thus no major differences in microstructure can be expected between terrestrial and Skylab processed M553 spheres due to convection. This conclusion was affirmed by detailed microstructural analyses (Ref. 27).

ACKNOWLEDGEMENT

REFERENCES

1. Brashears, M.R., and S. J. Robertson, "Research Studies on Materials Processing in Space Experiment M512 — Final Report," LMSC-HREC TR D306954, Lockheed Missiles & Space Company, Huntsville, Ala., December 1973.

2. Bourgeois, S. V., "Convection Effects on Skylab Experiments M551 and M553 — Phase C Report," LMSC-HREC TR D306955, Lockheed Missiles & Space Company, Huntsville, Ala., December 1973.

3. Bourgeois, S. V., and M. R. Brashears, "Fluid Dynamics and Kinematics of Molten Metals in the Low Gravity Environment of Skylab," AIAA Paper 74-205, presented at the AIAA 12th Aerospace Sciences Meeting, Washington, D. C., January 1974.

4. Fleming, M. C., Solidification Processing, McGraw-Hill, New York, 1973, pp. 154-155.

5. Kattamis, T. Z., "Nickel-Silver Alloy Evaluation, M553 Sphere Forming Experiment," University of Connecticut, Storrs, 4 December 1973.

6. Roshko, A., "On the Development of Turbulent Wakes from Vortex Wakes," NACA TN 2913, 1953.

7. Beer, S. Z. (Ed.), Physics and Chemistry of Liquid Metals, Marcel-Dekker, Inc., New York, 1972.

8. Taneda, S., "Experimental Investigation of Vortex Streets," J. Phys. Soc. Japan, Vol. 20, 1965, p. 1714.

9. Shair, F. H. et al., "The Effects of Confining Walls on the Stability of the Steady State Wake Behind a Circular Cylinder," J. Fluid Mech., Vol. 17, 1963, p. 546.

10. Papaulios, D., and P. S. Lyondis, "Turbulent Vortex Street and the Entrainment Mechanism of the Turbulent Wake," J. Fluid Mechanics, Vol. 67, Part I, 1974, p. 11.

11. Konkol, P. J., P. M. Smith, C. F. Willebrand and L. P. Connor, "Parameter Study of Electron-Beam Welding," Welding J., November 1971, p. 772.

12. Tong, H., and Geidt, W. H., "A Dynamic Interpretation of Electron Beam Welding," Welding J., June 1970, pp. 259s-266s.

13. Anonymous: Vapor Pressure Data, RCA Review, December 1962, pp. 571-576.

14. Beer, S. Z., Liquid Metals Chemistry and Physics, Marcel-Dekker, Inc., New York, 1972.

15. Metals Handbook, No. 8, American Society for Metals, Metals Park, Ohio, Vol. I, 1973.

16. Taylor, J. W., "Wetting by Liquid Metals," in Solid State Physics and Physical Metallurgy.

17. Laudise, R. A., J. R. Carruthers and K. A. Jackson, "Crystal Growth," in Annual Review of Materials Science, Vol. I, 1971, pp. 253-256.

18. Laudise, R. A., The Growth of Single Crystals, Prentice-Hall, Englewood Cliffs, N. J., 1970, pp. 86-103.

19. Goldak, J. A., G. Burbidge and M. J. Bibby, "Predicting Microstructure from Heat Flow Calculations in Electron Beam Welded Eutectoid Steels," Can. Met. Quart., Vol. 9, 1970, p. 459.

20. Cole, G. S., "Transport Processes and Fluid Flow in Solidification," in Solidification, American Society for Metals, Metals Park, Ohio, 1971, pp. 201-274.

21. Churchill, S. W., and J. D. Hellums, "Dimensional Analysis and Natural Convection," Chem. Engr. Prog. Symp. Ser., Vol. 57, 1964, p. 75.

22. Ostrach, S., "Role of Analysis in the Solution of Complex Problems," Third Intl. Heat Trans. Conf., Chicago, August 1966.

23. Melcher, J. R., "Discussions on Electrohydrodynamic Applications in Space Processing," Marshall Space Flight Center, Huntsville, Ala., 11 June 1973.

24. Sozou, C., "On Fluid Motions Induced by An Electromagnetic Field in a Liquid Drop Immersed in a Conducting Fluid," J. Fluid Mech., Vol. 51, 1972, pp. 585-591.

25. Melcher, J. R., and G. I. Taylor, "Electrohydrodynamics: A Review of the Role of Interfacial Shear Stresses," Ann. Rev. Fluid Mech., Vol. 1, 1969, p. 111.

26. Bupara, S. J., "Spontaneous Movements of Small Round Bodies in Viscous Fluids," Ph. D. thesis, University of Minnesota, Minneapolis, November 1964.

27. Bourgeois, S. V., "Solidification Theory for Skylab Experiments M551, M552 and M553 — Summary Report," LMSC-HREC TR D390140, Lockheed Missiles & Space Company, Huntsville, Ala., January 1974.

Table 1 - Comparison of Theoretical and
Experimental Bead Spacing

M551 Mtls.	Temp. T (°K)	Reynolds Number R	Strouhal Number S	Shedding Freq. f (Hz)	Theor. Bead Spacing λ (cm)	Flight Bead Spacing λ (cm)	Ground Bead Spacing λ (cm)
321 SS	1700	35	—	—	—	0.356	0.418
	2253	72.5	0.15	1.61	1.0		
2219 Al	916	50	—	—	—	—	—
	2113	171	0.185	1.98	0.81		
Ta	3270	121	0.175	1.88	0.86	1.57	0.94
	3833	181	0.188	2.02	0.80		

Table 2 - Comparison of Theoretical and Experimental
Shedding Frequency

M551 Material	Theoretical Shedding Frequency (Hz)	Flight Shedding Frequency (Hz)	Ground Shedding Frequency (Hz)
321 Stainless Steel	1.61	4.52	3.85
2219 Aluminum	1.98	—	—
Tantalum	2.02	1.03	1.71

Skylab

Ground-Base

Mag. 10X
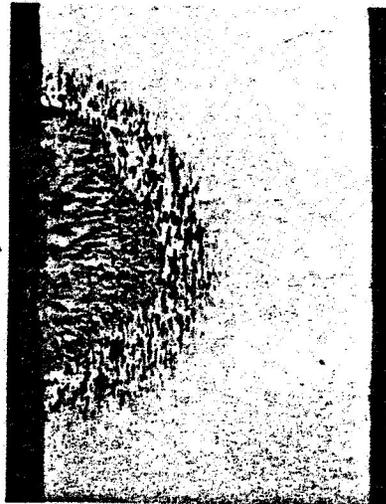
Cross Sections Pos. 5

Mag. 100X

Root of Electron Beam Weld
Nugget Showing Fine,
Equiaxed Grains

Root of Electron Beam Weld
Nugget Showing Banding and
Columnar Grain Growth

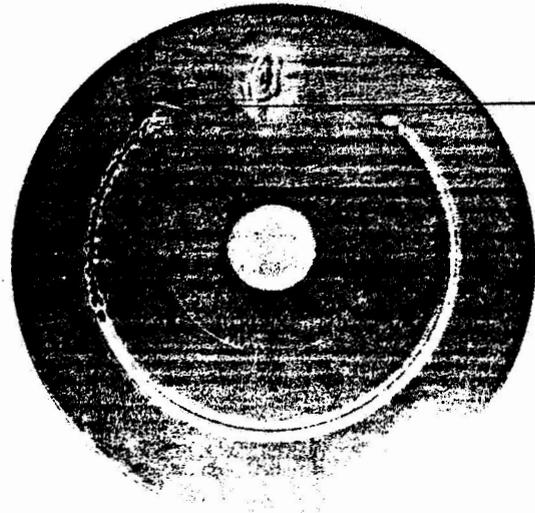Fig. 1 - Comparison of M551 Ground and Skylab 2219 Aluminum Microstructures

241
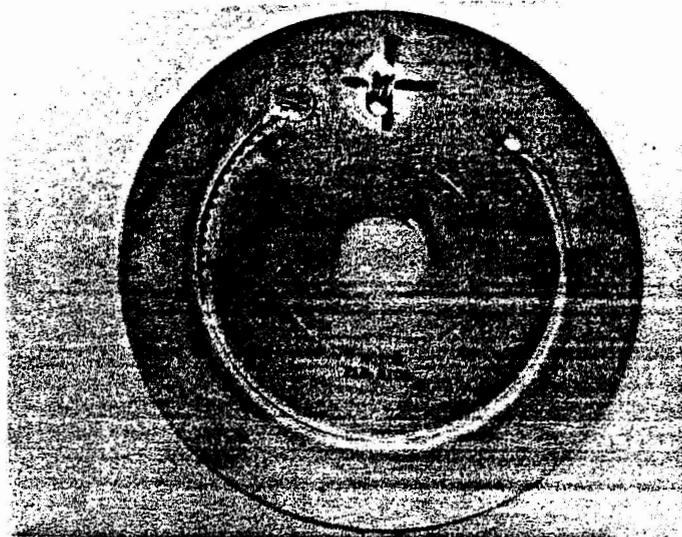

Fig. 2a - Stainless Steel Disk After M551 Flight Tests

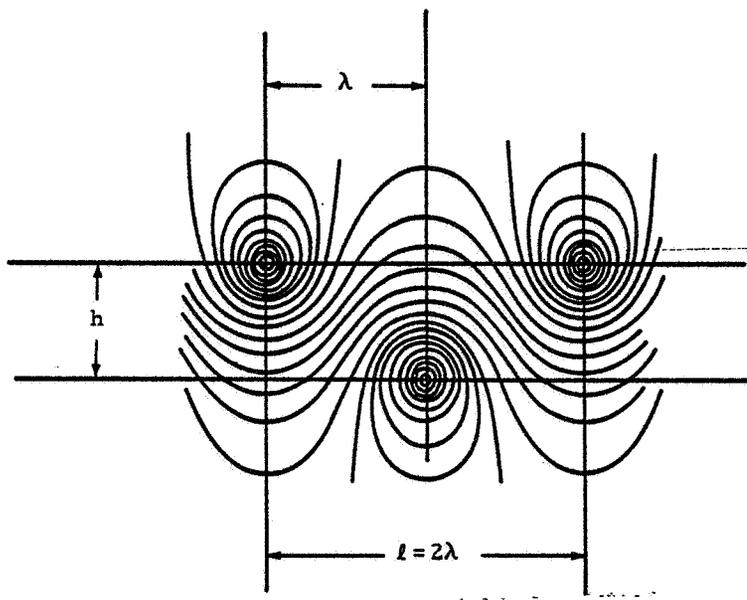Fig. 2b - Stainless Steel Disk After M551 Ground Tests

Fig. 3 - Kármán Vortex Street (Diagrammatic); Streamlines
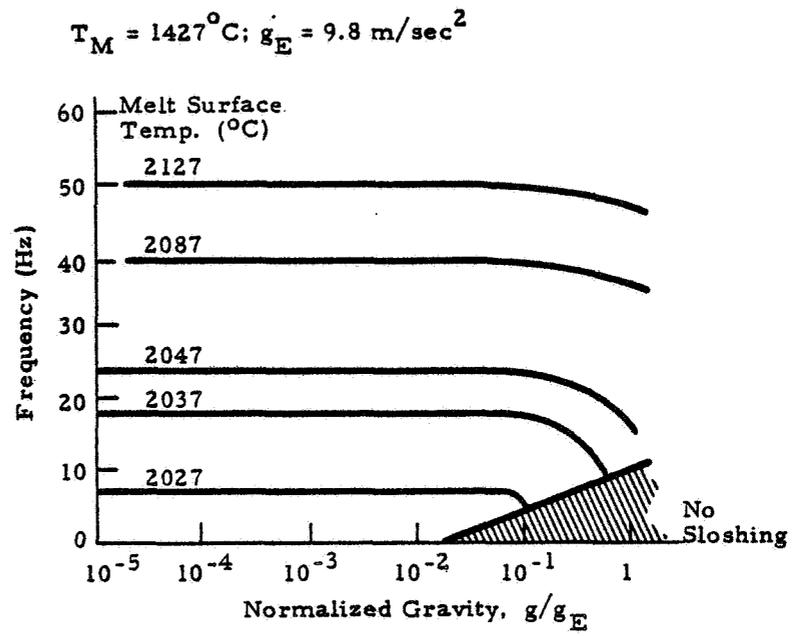Drawn in a System of Coordinates Moving with the
Vortex Street

$$T_M = 1427^{o}C; \quad \dot{g}_E = 9.8 \ m/sec^2$$

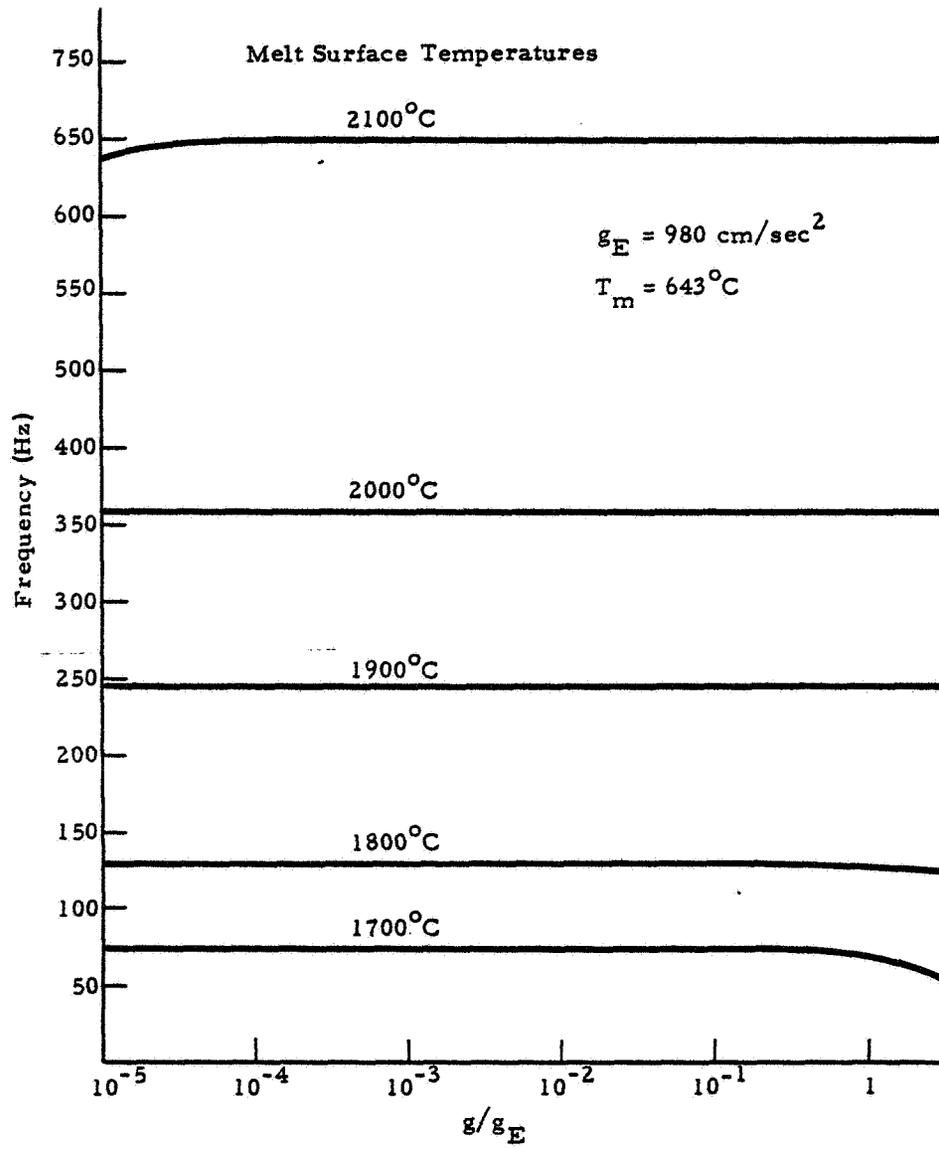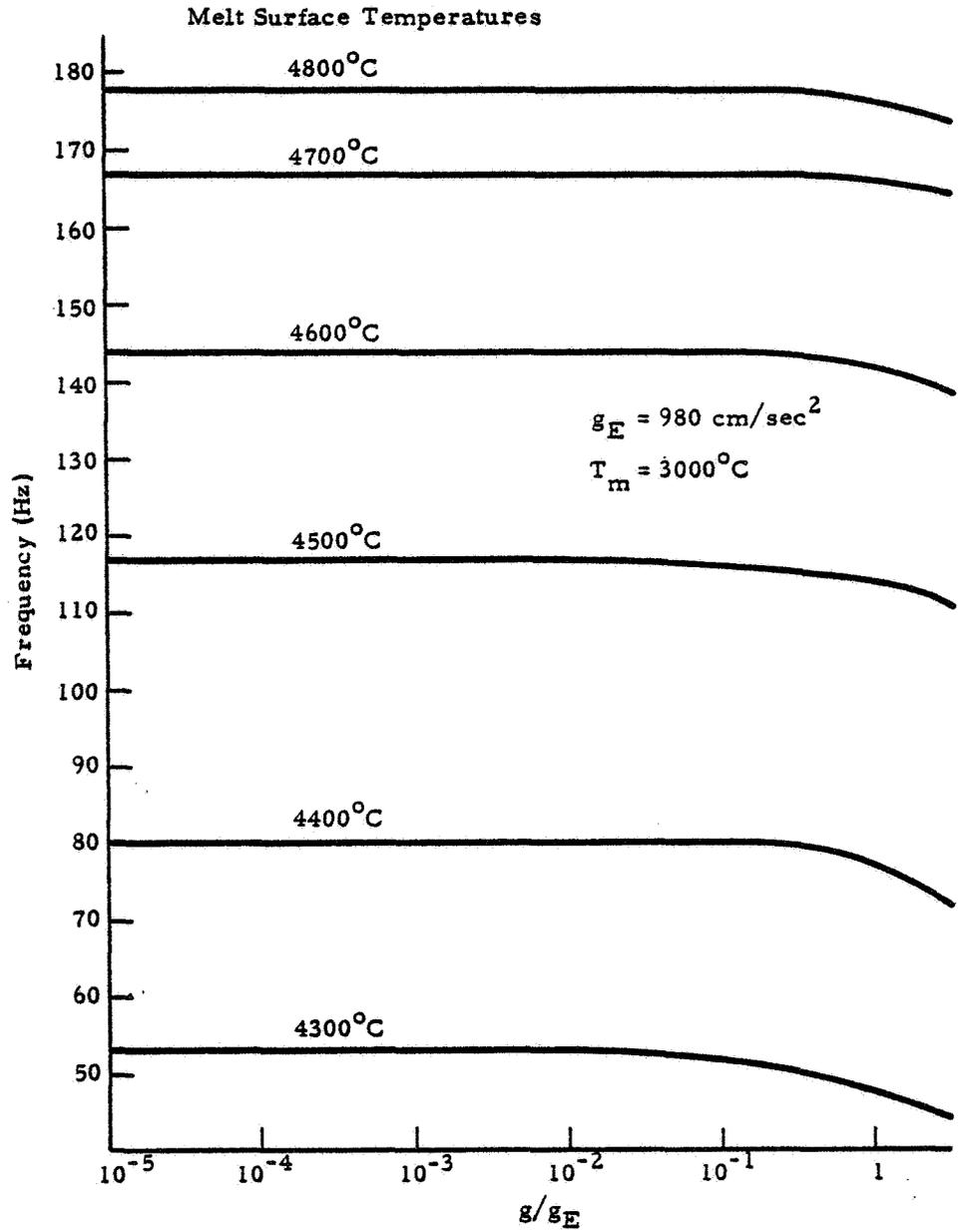Fig.4 - Spiking Frequency Graph of Stainless Steel

Fig. 5 - Spiking Frequency of Aℓ2219

Fig. 6 - Spiking Frequency Graph of Tantalum